Dalton Transactions

Accepted Manuscript

This is an *Accepted Manuscript*, which has been through the Royal Society of Chemistry peer review process and has been accepted for publication.

Accepted Manuscripts are published online shortly after acceptance, before technical editing, formatting and proof reading. Using this free service, authors can make their results available to the community, in citable form, before we publish the edited article. We will replace this *Accepted Manuscript* with the edited and formatted *Advance Article* as soon as it is available.

You can find more information about *Accepted Manuscripts* in the Information for Authors.

Please note that technical editing may introduce minor changes to the text and/or graphics, which may alter content. The journal's standard Terms & Conditions and the Ethical guidelines still apply. In no event shall the Royal Society of Chemistry be held responsible for any errors or omissions in this *Accepted Manuscript* or any consequences arising from the use of any information it contains.

ROYAL SOCIETY OF CHEMISTRY

www.rsc.org/dalton

Gold nanoparticles decorated graphene sheet-polypyrrole based nanocomposite: Synthesis, characterization and genosensing application

Ida Tiwari*, Mandakini Gupta[1], Chandra Mouli Pandey[1], Vandini Mishra
Centre of Advanced Study, Department of Chemistry, Faculty of Science,
Banaras Hindu University, Varanasi -India

ABSTRACT

We herein report the synthesis of gold nanoparticles (GNPs) decorated-graphene sheets (GO-GNPs) with the template of graphene oxide (GO) by a one-pot solution-based method. Polypyrrole-GO decorated GNPs nanocomposite (GO-GNPs/PPY) has been electropolymerized using potentiodynamic method on indium tin oxide (ITO) coated glass substrate. The as-synthesized nanocomposites are characterized by transmission electron microscopy, energy dispersive X-ray spectroscopy, scanning electron microscopy, thermogravimetric analysis, Fourier transform infrared and Raman spectroscopy. It has been found that GNPs of ca. 5 nm are uniformly dispersed on the surface of GO, and hold a high electrochemical active surface area. The surface morphology studies shows that PPY changes from nanoflowers to nanostars and then to nanosheets with increase in the scan rate (20-200 mV/s). The prepared GO-GNPs/PPY/ITO electrode was further used as genosensor where the electrochemical response was measured using methylene blue (MB) as a redox indicator. The genosensor shows the response time of 60 s with high sensitivity (1×10^{-15} M) and linearity (1×10^{-15}–1×10^{-6} M) with the correlation coefficient of 0.9975.

.

Keywords: Graphene, gold nanoparticles Polypyrrole, Electropolymerization, Genosensor

*** Corresponding author E-mail address: *sensorsbhu@yahoo.co.in,**
Phone: +91-5426702444, fax no.: +91-5422368174
[1]These authors contributed equally to this work.

Dalton Transactions Accepted Manuscript

INTRODUCTION

Conducting polymers (CPs), such as polypyrrole (PPY) has got enormous attention due to its strong electrical properties, ease of preparation and good environmental stability, which enable its wide application in electronic devices, electrodes for rechargeable batteries and supercapacitors, solid electrolytes for capacitors, sensors and corrosion protection materials.[1-5] Electrochemical polymerizations of pyrrole directly onto a substrate are reported to be rather kinetically controlled process than chemical polymerization.[6-7] Dubal et al. reported the formation of nanobelts, nanobricks and nanosheets of PPY at different scan rates on the pure stainless steel foil where the NO_3^- acts as a dopant.[8] Qu et al. discuss the preparation of PPY microstructures at stainless steel surface with (+) and (-) camphorsulphonic acid as dopant.[9] Similarily, microtubules of polypyrrole were also synthesized by an electrochemical template-free method in the presence of β-naphthalenesulfonic acid as a dopant by Yang et al.[10] Horn-shaped PPY was prepared using pulse potentiometry technique by Wang et al.[11] PPY was found to be compatible material for the immobilization of DNA probes where the DNA was used as dopant for PPY.[12] Inspite, of the several interesting properties, the major drawback is the insolubility of this conducting polymer in common solvents and infusibility which make them poorly processable either via a solution technique or by melt-processing methods. These material properties can be improved by forming either pyrrole copolymers or PPY composites or blends with commercially available polymers or inorganic materials, which offer better mechanical and optical properties as well as stability and processability. In this context, graphene oxide (GO) due to its excellent inplane mechanical and thermal properties, outstanding electrical conductivity and cost effectiveness has been widely explored as a composite material with PPY.[13] The presence of oxygen-containing functional groups, such as hydroxyl, epoxide, carbonyl, carboxyl, etc., makes GO hydrophilic in nature which helps it to interact with solvents. Although, GO posses above mentioned properties, they are electrically insulating in nature due to presence of these functional groups and in order to obtain high electrical conductivity it is necessary to reduce graphene oxide.[14] As, PPY has been reported to be able to act as reducing agents to reduce GO to graphene, thus it eliminates the need for pre or post electrochemical reducing step and also eliminates the possibility to deal with hazardous chemicals like hydrazine which is normally reported to reduce GO.[3] Moreover, using GO as starting material avoids aggregate formation in solvent during PPY composite processing, where the PPY not only reduces the GO

Dalton Transactions Accepted Manuscript

but also gets intercalated between the GO sheets and helps in the better dispersion of GO into the electropolymerized PPY film. Hence, being cost effective nanomaterial graphene and their derivatives can act as better substitute for reinforcement or as filler material for the preparation of polymer based nanocomposite replacing carbon nanotubes.[3] Till date several researches have been carried out based on graphene/PPY composites using both chemical[1,13,15] and electrochemical route[16-17] utilizing various dopants. Moreover, several reports are also available to utilize GO/PPY composite for different applications including supercapacitor[18], fuel cell[19,16], solid phase microextraction of phenol,[20] but very few reports available in the literature on biosensor application.

It is reported that nanocomposites based on metal nanoparticles and exfoliated graphene nanosheet (GR) with synergistic effect have exhibited particular promise in biosensing characteristics as they can play very interesting and enhanced signal because of its fast electron transfer and large working surface area.[21] In this context, gold nanoparticles (GNPs) are well known to have unique properties such as high surface free energy, good adsorption property, good conductivity, biocompatibility and excellent catalytic properties which make them a suitable material in the field of sensor as they can greatly enhance the current response and help in improving the sensor performance.[22] Recently, GNPs was used in DNA hybridization sensing as it acts as catalyst for the amplification of signal produced due to biochemical reaction (DNA hybridization).[23]

A lot of research has been carried out in the area of DNA diagnostics due to its application in various fields such as gene analysis, identification of genetic disorders, tissue matching, pharmacogenetics, food safety and forensic sciences.[24-25] Electrochemical DNA biosensors are well suited for rapid and direct detection of DNA because of its ease of handling, miniaturization, and microelectronic integration and the basic principle of working involves the recognition of specific DNA sequences.[26-28] For the construction of electrochemical DNA biosensors, immobilization of DNA on the suitable surface is required so that the stability of DNA gets improved which can further ensure the interaction of the probe DNA and the target DNA.

Taking all the above precedence into account, we have prepared GNPs decorated GO-PPY nanocomposite (GO-GNPs/PPY) where GO-GNPs act as a reinforcement material and help in the immobilization of biomolecule while PPY act as matrix material for the dispersion of

Dalton Transactions Accepted Manuscript

nanoreinforement and their synergism provides improved property to nanocomposite. This prepared material was used for the fabrication of DNA biosensor for the detection of coliforms (*Escherichia coli* O157:H7).

RESULTS AND DISCUSSION

The PPY nanostructures formation by potentiodynamic method depends on the scan rates of deposition as reported earlier.[32] Taking this phenomena into consideration, PPY nanostructures formation was first studied by cyclic voltammetry (CV) cycling from 0 to +1.2 V vs. Ag/AgCl at different scan rates without addition of GO and GO-GNPs nanostructures. Fig. 1 shows the SEM images of pure PPY thin films deposited on ITO at different scan rates, (a) 20 mV/s, (b) 50 mV/s, (c) 100 mV/s, (d) 200 mV/s. From the micrographs, it has been observed that the surface morphology of PPY changes from agglomerated nanoflowers to nanostars and then to nanosheets with increase in the scan rate. The surface of PPY films deposited at 20 mV/s scan rates [Fig.1 (a)] shows some agglomerated regularly arranged nanoflowers like structure along with nanocubes. At 50 mV/s scan rates, the PPY film looks like nanostar type structure [Fig. 1 (b)] which further appeared like interconnected nanobricks like structure at higher magnification [inset to Fig.1 (b)]. Further increase in scan rates upto 100 mV/s [Fig.1 (c)] causes the formation of hierarchical nanosheets which further form the PPY nanospheres decorated PPY nanosheets as the scan rates increased from 100 to 200 mV/s [Fig. 1 (d)]. The probable reason behind formation of these nanostructures at different scan rates might be the deposition time. The time for deposition and dissolution of polymer become shorter at higher scan rates leading to the formation of nanosheets while the slow scan rates provides more time for deposition, hence dense and packed structures are formed.[32] For the further preparation and characterization of GO-GNPs/PPY hybrid nanocomposite, scan rates 50 mV/s (deposition of 10 cycles in thickness) was used in all this experimental work as the film forming ability was observed to be good. Fig. 2 (a) and (b) shows the scanning electron micrograph of pure PPY and GO-GNPs/PPY hybrid nanocomposite at 50 mV/s scan rates respectively which do not show any particles on the PPY structure [Fig. 2 (a)] while the Fig. 2 (b) depicts the formation of interconnected nanoribbons like structures with some nanoparticles which is proposed to be due to the polymerization of PPY over the GO-GNPs template. Further, after immobilization of pDNA onto GO-GNPs/PPY electrode shiny and globular morphology is observed (Fig. 2 (c)) showing the covalent binding of the probe DNA onto GO-GNPs/PPY electrode.

Dalton Transactions Accepted Manuscript

Fig. 3 (a), (b) and (c) represents the TEM image of prepared materials PPY, GO-GNPs, and GO-GNPs/PPY respectively. The TEM micrograph of PPY surface are rough and compact (*cf.* Fig.3a) in nature with amorphous diffraction pattern (inset to Fig. 3a), the GNPs with the particle size of about 13 nm were well separated on wrinkled graphene sheets (Fig.3 b) with the diffraction pattern showing crystalline nature (inset to Fig. 3b) and the GO-GNPs/PPY hybrid nanocomposites showing uniform distribution of PPY over GO-GNPs (Fig.3 c). The diffraction pattern of GO-GNPs/PPY nanocomposite is shown as inset to Figure 3(c). The energy dispersive X-ray of the GO-GNPs/PPY nanocomposite also supports the formation of nanocomposite (Figure 3d).

Figure 4 displays the FTIR spectra of (i) GO, (ii) GO-GNPs, (iii) PPY and (iv) GO-GNPs/PPY respectively. GO shows the characteristic absorption bands of oxide groups, such as C=O stretching vibration at 1733 ν_{max}/cm^{-1} and alkoxy (C-O) stretching at peak 1076 ν_{max}/cm^{-1} and C=C stretching at 1619 ν_{max}/cm^{-1} . Compared to GO, no probable change has been observed for GO-GNPs. Curve iii shows the characteristic peaks of PPY at 3441 ν_{max}/cm^{-1}, 1533 ν_{max}/cm^{-1} , 1384 ν_{max}/cm^{-1}, 1161 ν_{max}/cm^{-1} and 1034 ν_{max}/cm^{-1} due to -NH stretching, -C=C stretching, -C-N stretching with -C-C bending, -C=N stretching and -N-H bending. On comparing peaks of GO, GO-GNPs and PPY, we observed that the peak due –C=O stretching within GO-GNPs/PPY nanocomposite downshifted to 1633 ν_{max}/cm^{-1} which may be due to π-π interaction and H-bonding between GO-GNPs layers and aromatic polypyrrole rings and also suggesting that –C=O efficiently act as dopant during polymerization[31] and the formation of the nanocomposite is also confirmed by the presence of the peak at 1384 ν_{max}/cm^{-1} due to –C-N stretching vibration and shifting in peaks in the range of 1100-800 ν_{max}/cm^{-1}.

The thermal stability of the GO film, GO-GNPs, pure PPY and the GO-GNPs/PPY composite are shown in Fig. S1(a). The mass loss for all the samples at 100^0 C was due to the removal of absorbed water. Thermal decomposition of the GO sheets (curve i) from 100^0 C to 240^0 C was due to the removal of labile oxygen functional groups, and the weight loss at 240^0 C onwards was due to the GO reaching its deflagration point and the solid decomposing into carbon soot.[33] The thermal decomposition of GO-GNPs are similar to GO sheets but showing more stable nature of the system as can be seen from the Fig. S1 (a) (curve ii). The weight of the PPY film remained around 87% at 275^0 C, and then gradually decreased and the figure also

Dalton Transactions Accepted Manuscript

shows that the PPY prepared by electropolymerization are stable in nature (curve iii). The GO-GNPs/PPY film showed a similar pattern of weight loss in the range of 275 to 600^0 C (curve iv). Fig. S1 (b) represents the DTA analysis of GO film (curve i), GO-GNPs (curve ii), pure PPY (curve iii) and the GO-GNPs/PPY composite (curve iv). The figure shows an exothermic peak at 229^0 C in both GO and GO-GNPs due to the labile oxygen functional groups but the intensity of this peak is lower in GO-GNPs, shows the better stability of GO-GNPs. The DTA curves of PPY and GO-GNPs/PPY nanocomposite have similar pattern. Thus, the hybridization of GO-GNPs and PPY is also supported by TGA and DTA analysis, where the profile of the composite lays between the profiles of GO, GO-GNPs and PPY. It is proposed that the similarities in TGA and DTA profile between PPY and GO-GNPs/PPY is due to uniform dispersion of GO-GNPs in the PPY matrix.[34]

Figure S2 shows the Raman spectra of GO, GO-GNPs, PPY and GO-GNPs/PPY nanocomposite. In Raman spectra of GO (curve i), two prominent peaks appear at 1642 cm^{-1}, and 1366 cm^{-1}. The peak at 1642 cm^{-1} appears due to in plane bond stretching motion of pairs of C sp^2 atom (the first order scattering of the E_{2g} photon) called as G band while the peak at 1366 cm^{-1} is due to D band which arises from sp^3 bonded carbon atom indicating disorder in the structure.[35] This D mode is forbidden in perfect graphite and only becomes active in presence of disorders. Here the I_D/I_G (intensity ratio of D and G band) ratio was found to be 0.831. In the Raman spectrum of the GO-GNPs nanocomposite (curve ii), G band and D band are shifted to 1592 and 1347 cm^{-1} respectively, implying that graphene main structure is retained. Both the peaks were broadened and I_D/I_G was found to be 0.846 in the GO-GNPs nanocomposite. The significant increase in value of I_D/I_G shows the decrease in the average size of the sp^2 domains and partially disordered structure of graphene nanosheets which may be caused by the interaction of GO and GNPs.[36-37] Further, no peaks were observed for GNPs or it appears in very low intensity (curve iii). The PPY shows two strong bands, one broad band at 1327 cm^{-1} which is attributed to the ring stretching and N-H in-plane deformation of oxidized (doped) species and the other band at 1565 cm^{-1} (curve iv) is due to backbone stretching mode of C=C bonds.[38] The Raman spectrum of GO-GNPs/PPY hybrid nanocomposite (curve v) confirms the formation of GO-GNPs/PPY nanocomposite.

Dalton Transactions Accepted Manuscript

Contact angle (CA) measurements (Fig. S3) were carried out using the sessile drop method. The results show that after the electrodeposition of GO-GNPs/PPY on ITO electrode there was a decrease in the CA from 80.2^{o} [Fig. S3, image (i)] to 54.8^{o} [Fig. S3, image (ii)] showing hydrophilic groups were introduced on the surface of ITO. The decrease in CA may be due to the introduction of GO having polar groups –COO^{-} which increases the hydrophilicity of the electrode surface. A further decrease [Fig. S3, image (iii)] in CA (28.52^{o}) after the immobilization of pDNA onto GO-GNPs/PPY/ITO electrode was observed which may be due to enhancement of hydrophilicity caused by the presence of negatively charged phosphodiester backbone of DNA.

The conductivity of the film was measured using the four points probe technique with a low current source (LCS- 02), digital microvoltmeter (DMV-001) and PID controlled oven. PPY deposited on ITO electrode shows conductivity of 0.042 S cm^{-1}. Whereas, for GO/PPY/ITO electrode an increase in the conductivity was obtained (0.106 S cm^{-1}) which further gets increased to 0.198 S cm^{-1} for the GO-GNPs/PPY/ITO electrode. This increase in conductivity may perhaps be due to the increase in the charge-carrier density owing to the presence of GNPs and GO.[39-40] The electrochemical characterization of GO-GNPs/PPY electropolymerized film on ITO electrode have been investigated by CV technique in phosphate buffer (50mM, pH 7.0, 0.9% NaCl) containing 5 mM $K_3[Fe(CN)_6]^{3-/4-}$]. The effect of pH on the performance of pDNA/ GO-GNPs/PPY/ITO bioelectrode has been investigated between ranges 6.0 to 8.0 at 50 mV/s. The current response has been found to be maximum at pH 7.0 (data not shown). The high response current obtained at pH 7.0 indicates that pDNA/GO-GNPs/PPY/ITO bioelectrode is more active at pH 7.0 at which DNA retain its biological activity. Thus all the experiments have been conducted at pH 7.0 at 25 ^{o}C. Fig. S4 exhibits the cyclic voltammogram of GO-GNPs/PPY/ITO electrode as a function of scan rate (10–300mV/s; curves i-xiv). The anodic and cathodic peak potentials were observed to be 0.202 V and 0.042 V. The peak separation (ΔE) was found to be 0.160 V. The anodic and cathodic peak currents (i_{pa} and i_{pc}) exhibit a linear relationship with square root of sweep rate [inset (i), Fig. S4], suggesting that the electrochemical reaction is diffusion-controlled and follows Eqs.(1) and (2).[41] The peak potential (E_a and E_c) increases as a function of the scan rate [inset (ii), Fig. S4], indicating facile charge transfer kinetics, and follows Eqs. (3) and (4)

Dalton Transactions Accepted Manuscript

I_{pa} (A) [pDNA/GO-GNPs/PPY/ITO] = 0.0910 x 10^{-3} (A) +0.614 x 10^{-3}A (s/mV) [scan rates (mV/s)]

R^2 = 0.9982, SD = 0.0161 x 10^{-4} ……..(1)

I_{pc} (A) [pDNA/GO-GNPs/PPY/ITO] = - 0.179 (A) –0.0448 A (s/mV) [scan rates (mV/s)]

R^2 = -0.9905, SD = 0.0273 x 10^{-4} ……. (2)

E_a (V) [pDNA/GO-GNPs/PPY/ITO] = 0.0676 (V) + 0.107 (V) x log [scan rates]

R^2 = 0.9945, SD = 0.0034…….. (3)

E_c (V) [pDNA/GO-GNPs/PPY/ITO] = -0.163 (V) - 0.976 (V) x log [scan rates]

R^2 = -0.9861, SD = 0.0054 …… (4)

$$\ln k_s = \alpha \ln (1-\alpha) + (1-\alpha) \ln \alpha - \ln (RT \ln F\nu) - \alpha (1-\alpha) n F \Delta E_p/RT \quad (5)$$

where R and SD are the correlation coefficient and standard deviation, respectively. The transfer coefficient α was calculated from the slope of Laviron's plot and the charge transfer rate constant (k_s) was calculated using equation (5) and observed to be 0.51 and 3.87 s^{-1} respectively.[42] For calculating the total surface concentration of pDNA on GO-GNPs/PPY/ITO, slope was calculated using Laviron's plot (inset ii to Fig. S4). The slope is given by following equation:

$$RT/\alpha n F = 0.1253 \quad (6)$$

$$I_p = n^2 F^2 \nu\tau A (4RT)^{-1} \quad (7)$$

where i_p/ν has been calculated from the slope of i_p vs. ν plot. The total surface concentration of pDNA has been found to be as 1.542 x 10^{-11} mol cm^{-2} indicating high surface coverage of pDNA onto the GO-GNPs/PPY/ITO electrode.

The electrochemical studies of PPY/ITO, GO/PPY/ITO, GNPs/PPY/ITO GO-GNPs/PPY/ITO electrode, and pDNA/GO-GNPs/PPY/ITO bioelectrode are compared in Fig.5. The CV of PPY/ITO electrode (i) displays the sharp anodic and cathodic redox peaks at the potential of 0.232 V and -0.0075 V having anodic and cathodic peak currents of 3.460 x 10^{-4} and 4.386x 10^{-4} A respectively. However, GNPs/PPY/ITO (curve ii, 4.52 x 10^{-4} and 4.75 x 10^{-4} A)

Dalton Transactions Accepted Manuscript

and GO/PPY/ITO (curve iii, 4.692 x 10^{-4} to 5.526 x 10^{-4} A) electrode exhibits increased anodic and cathodic peak currents while GO-GNPs/PPY/ITO electrode shows further increase in currents (curve iv, 7.887 x 10^{-4} A and 7.411 x 10^{-4} A) with no appreciable change in potential. The increase in peak currents clearly indicates that, the addition of GNPs, GO and GO-GNPs to the PPY nanocomposite modified ITO act as a catalyst to promote electron transfer across the electrode[43] and finally results in increased current density. On immobilization of pDNA, there was a sharp decrease in the peak currents (curve v, 3.097 x 10^{-4} A and 3.353 x 10^{-4} A) with the increase in peak potentials with respect to that of the GO-GNPs/PPY/ITO electrode have been observed. This probably is due to the repeating structure of phosphate backbone which makes the DNA molecules electronegative and thus repulse the $[Fe(CN)_6]^{3-}$. The other reason behind this phenomenon may be attributed to the long polymer chain of DNA which may experience steric hindrance, and further reduces the electron transport rate resulting in the sluggish electron transport across the bioelectrode.[42]

Biosensing Studies

Optimization of the pDNA on the GO-GNPs/PPY/ITO surface has been conducted by varying the pDNA concentration from 10^{-5} M to 10^{-10} M to avoid any non-specific adsorption of the cDNA. As shown in Fig. S5**,** the peak current get leveled off at 1 μM pDNA concentration where the optimum probe density was found to be 3.2×10^{13} cm^{-2}. Hence 1 μM concentration of pDNA was used throughout the experiment, presuming that at this concentration maximum immobilization is achieved. Figure S6 (a) shows results of the differential pulse voltammetric (DPV) studies for detection of hybridization. The curves (i) GO-GNPs/PPY/ITO, (ii) GO/PPY/ITO, (iii) GNPs/PPY/ITO and (iv) PPY/ITO are the DPV response obtained after immobilization of pDNA on the electrodes and after hybridization the response obtained are shown as curves (v) at pDNA/PPY/ITO, curve (vi) at pDNA/GNPs/PPY/ITO, curve (vii) at pDNA/GO/PPY/ITO and curve (viii) at pDNA/GO-GNPs/PPY/ITO bioelectrodes, using methylene blue (MB, 20 μM) as redox hybridization indicator. As reported earlier MB can be used to differentiate between hybridized and unhybridized DNA because the MB has capability to bind with the unpaired nitrogenous bases of single-stranded DNA and undergo reduction by oxidizing the unpaired nucleosides bases as compared to double-stranded DNA.[44-46] It has been observed that the peak current after hybridization was very low for pDNA/GO-GNPs/PPY/ITO bioelectrode showing maximum hybridization efficiency of complementary DNA with

Dalton Transactions Accepted Manuscript

pDNA/GO-GNPs/PPY/ITO bioelectrode. Further, various target probe of concentrations (1 x 10^{-15} M to 1 x 10^{-6}) were used for the biosensing studies at 25 ^{o}C (Fig.6a). It has been observed that incubation time of 60 s is sufficient for the interaction of MB with pDNA/GO-GNPs/PPY/ITO bioelectrode as discussed earlier. As indicated in Fig.6 (a) current signal of MB reduction decreases as the target concentration increases upto 1 x 10^{-6} M and remains constant with further increase in the cDNA concentration after incubation with cDNA sequence, which shows that the entire immobilized probe DNA is involved in hybridization process at the bioelectrode surface. Fig. 6 (b) indicates that the peak current of MB reduction follow linear relationship with the logarithm of concentration of target DNA. The peak current increases as the concentration of target cDNA decreases and follow the relation as indicated in Eq. (8)

$$I_{dsDNA/PPY/GO\text{-}GNP/ITO}\ (A) = -1.5510 \times 10^{-7}\ (A)\ [\log(\text{target DNA concentration})] + 2.8124 \times 10^{-7} \quad (8)$$

The detection limit of the biosensor was found to be 1 x 10^{-15} M which is higher in comparison to pDNA/GO/PPY/ITO bioelectrode (1 x 10^{-13} M; Fig. S6 (b)) and other reports in literature [ST 1].[47-54] The experiment was repeated for 5 times to check the repeatability of the result produced and the imprecision of the data as indicated by the error bars was found to be within 3%.

Further, the effect of cDNA, ncDNA and obmDNA on probe DNA/GO-GNPs/PPY/ITO bioelectrode (Fig.S7). It was observed that after interaction of cDNA with probe DNA, a significant decrease in the peak current compared to probe DNA has been achieved which is indication of indicates the hybridization of probe DNA with complementary DNA. This decrease is peak current is associated with the unavailability of nitrogenous base to oxidize as compared to frequent availability of nitrogenous base in case of pDNA. On the other hand, incubation of pDNA/GO-GNPs/PPY/ITO bioelectrode with ncDNA, no appreciable change in MB reduction current was noticed. After, incubating the electrode with obmDNA a significant decrease in MB reduction peak, as compared to that of the non-complementary DNA was observed, which indicates that the fabricated DNA sensor can discriminate even a single nucleotide variation in target DNA sequence.

Reusability and stability of the bioelectrode

It has been found that the pDNA/GO-GNPs/PPY/ITO bioelectrode can be used 5–6 times after regeneration (data not shown). For this purpose, the bioelectrode is immersed in buffer solution

Dalton Transactions Accepted Manuscript

(pH8.0) containing Tris–HCl (10mM) and EDTA (1mM) at 100° C for 5 min, followed by cooling in ice bath for about 30 min, which removes complementary DNA via thermal denaturation. The stability of the bioelectrode is analyzed by measuring response as a function of % reduction in current with respect to time. The observed % decrease in the current was found to be 7 % up to 58 days indicates stability of the bioelectrode as 7-8 weeks.

Electrochemical hybridization studies with real microbial samples

The specificity of the pDNA/GO-GNPs/PPY/ITO electrode has been studied with DNA culture samples of *K. pneumonia*, *Neisseria meningitides* and *S. typhimurium*. Fig. S8 shows decrease in the value of peak current after treating with *E. coli* samples indicating specific hybridization. Whereas on treating with DNA samples of other pathogens (*S. typhimurium*, *N. meningitides*, *K. pneumonia*), no significant change in the peak current with respect to the probe DNA was observed showing that the real samples of other pathogens have insignificant interference towards *E. coli* detection.

CONCLUSIONS

GNPs decorated graphene reinforced polymer nanocomposite has been synthesized by electrodynamic polymerization technique and characterization was performed by different techniques which reveal the formation of GO-GNPs/PPY nanocomposite. This fabricated platform was utilized to detect *E. coli* using DPV. The presence of gold decorated graphene along with conducting polymer polypyrrole not only increases the electron transfer on electrode surface but also help in the immobilization of the probe DNA. This platform could be further used for the onsite monitoring of the waterborne pathogens, coliforms.

EXPERIMENTAL SECTION

Reagents and materials

Graphite, gold chloride trihydrate ($HAuCl_4.3H_2O$), Sodium borohydride [$NaBH_4$ (95%)], Pyrrole and Sodium citrates dehydrate were purchased from Aldrich, USA. Pyrrole was distilled prior to use. All other chemicals employed were of analytical reagent grade, purchased from Sigma-Aldrich and were used as received. Probe sequence specific to *E. coli,* identified from the 16s rRNA coding region of the *E. coli* genome, complementary, non-complementary and one-base mismatch target sequences have been procured from Sigma Aldrich, Milwankee, USA.[42] All reagents and solutions were prepared in Millipore deionised water. The solution of

Dalton Transactions Accepted Manuscript

oligonucleotide are prepared in Tris–EDTA buffer (1M Tris–HCl, 0.5M EDTA) of pH 8.0 and stored at -20 ^{o}C prior to use.

Probe I: DNA probe (pDNA): Amine-5´-GGT CCG CTT GCT CTC GC-3´

Probe II: Complementary (cDNA): 5´-GCG AGA GCA AGC GGA CC-3´

Probe III: Non-complementary: 5´-CTA GTC GTA TAG TAG GC-3´

Probe IV: One-base mismatch: 5´-GCG AGA G**A**A AGC GGA CC-3´

Characterization

The electrochemical synthesis and cyclic voltammetric studies of GO-GNPs/PPY were performed with Autolab potentiostat/galvanostat (Eco Chemie, Netherlands). Three electrode system was used for recording cyclic voltammetry (CV), where modified indium tin oxide (ITO) electrode were employed as working electrode, an Ag/AgCl (3 M KCl) as reference electrode and Pt wire as counter electrode. All electrochemical measurements were carried out in 4 mL, 0.05 M phosphate buffer saline, pH 7.0 containing 5mM $[Fe\ (CN)_6]^{3-/4-}$ and deaerated by bubbling nitrogen for 15 minutes prior to the experiments. SEM of the electrochemically deposited materials on ITO electrode was performed with Quanta 200 FEI (13 kV). TEM of the prepared materials was performed with Technai 20 G^2 (200 kV). Raman spectra were recorded on a micro-Raman setup (Renishaw, UK) equipped with a grating of 2400 lines/mm and a peltier cooled CCD. TGA and DTA were performed by Perkin Elmer (STA 6000) in the temperature range of 30 ^{o}C-700 ^{o}C. Fourier transform infrared spectra (FTIR) were collected on Perkin Elmer (Spectrum Two) Fourier transform infrared spectrophotometer.

Preparation of GO-GNPs

Graphene oxide (GO) was prepared from natural flake graphite powder by the modified Hummers method.[29] and GO-GNPs has been prepared as reported with some modification.[30] In brief, 28 mg of GO and 200 µL of $HAuCl_4.3H_2O$ solution (2.5 mM) were dispersed in 28 mL water in a round bottom flask. For exfoliation of GO, ultrasonication was performed till the solution appears translucent with no visible particulate,[31] and then it was heated to 100 ^{o}C using condenser. Further then 50 µL each of sodium citrate dehydrate (3.4 mM) and sodium borohydtrate ($NaBH_4$, 2.5.mM) were added to this solution and stirred for at least 1 hour at 100° C. Then, prepared GO-GNPs was collected by centrifugation, washed with water 3-4 times and dried it in vacuum for 24 hrs.

Dalton Transactions Accepted Manuscript

Electrochemical polymerization and deposition of GO-GNPs/PPY nanocomposite

Prior to electropolymerization, the ITO electrode was hydrolyzed using $H_2O_2/NH_4OH/H_2O$ solution (1:1:5,v/v) for about 30 min at 80 ºC. GO-GNPs/PPY films were electrodeposited onto ITO for electrochemical characterization and also for surface characterization. In the typical experiment, 4 mL GO-GNPs aqueous dispersion (1 mg/mL) containing 0.5 M Pyrrole prepared in KNO_3 (0.1 M) ultrasonicated to form uniform mixture. For comparison, pure PPY films were synthesized from an electropolymerization solution containing 0.05 M pyrrole and 0.1 M KNO_3. Potentiodynamic deposition of GO-GNPs/PPY, GO/PPY hybrid nanocomposite and PPY was performed by CV scanning in the potential range of 0-1.2 V vs. Ag/AgCl at the scan rates of 50 mV/s.

Fabrication of pDNA/GO-GNPs/PPY/ITO bioelectrode

The bioconjugation of aminated probe DNA (pDNA) to the GO-GNPs/PPY/ITO electrode surface was performed using EDC-NHS as cross linker. To allow coupling between the amine terminal of pDNA and –COOH group of GO-GNPs/PPY/ITO, 20 µL of pDNA was spread onto the modified electrode surface followed by 5 h incubation in a humid chamber at room temperature (25^0C). The pDNA/GO-GNPs/PPY/ITO bioelectrode was further rinsed with Tris–HCl (10 mM) and EDTA (1 mM) buffer solution (pH 8.0) to remove any physically adsorbed pDNA on the electrode surface. The prepared pDNA/GO-GNPs/PPY/ITO bioelectrode were utilized for detection of *E. coli* by subjecting them to various concentrations of complementary target DNA for 60 s and the corresponding deference in peak current value was measured using DPV.

DNA hybridization study

The DNA hybridization was allowed to proceed for 60 s which was found to be sufficient for hybridization with target cDNA probes. The target-hybridized bioelectrodes has been carefully washed with phosphate buffer solution to remove unbound target molecules and are subject to the analysis of hybridization using DPV after pre-incubation in methylene blue (20µM) at +0.1V for 10 s. The control experiment was performed with samples containing same concentration of non-complementary (ncDNA probe) and one-base mismatch (obmDNA probe) sequences for 60 s at 25 ^{o}C. For sensing experiments, the DNA sequences were dissolved in appropriate volume of phosphate buffer (0.05 M, pH 7.0) to get stock concentration of about 100µM. This concentration is further diluted with phosphate buffer (0.05 M, pH 7.0) to obtain desired

Dalton Transactions Accepted Manuscript

concentrations of cDNA ranged from 10^{-6} M to 10^{-15} M. In the simulative experiment real sample analysis was done by using *E. coli* DNA sequence and the other steps were as mentioned above.

Extraction of DNA from bacterial clinical samples. The extraction of DNA has been conducted from a panel of strains comprising of *E. coli, K. pneumonia*, *Neisseria meningitides* and *S. typhimurium.* For this process, the suspensions of the colonies were vortexed by pouring it into 100 µl sterile MilliQ water. The suspension is boiled (10 minutes) and is centrifuged (10, 000 rpm; 5 min), followed by the addition of equal volume (100 µl) of 24:1 (v/v) chloroform: iso-amyl alcohol. The solution was further centrifuged at12000 rpm for 10 mins, which result in the formation of a layer above the solution containing DNA which was pipetted out and kept at -20°C prior to use.[53]

Pre-treatment of extracted DNA. All the bacterial clinical samples are prepared in Tris-EDTA buffer and are denatured by heating in a water bath (95°C) for 5 min and are immediately chilled in ice to obtain denatured single-stranded DNA. These aliquot of samples are subjected to sonication (15 min at 120 V) to break the long DNA strands into smaller fragments of the DNA.[55]

ACKNOWLEDGEMENTS

Authors are thankful to UGC for financial assistance. Authors are also thankful to Prof. O. N. Srivastava (BHU) for providing SEM and TEM facilities, Prof. B. Ray (Polymer Chemistry, Department of Chemistry) for double distillation of Pyrrole monomer. Prof. Ranjan Kumar (BHU) for Raman analysis and, Mr. Saurabh Kumar for conductivity measurement. Thanks are due to Dr. Gajjala Sumana (CSIR-NPL) and Prof. B.D. Malhotra for interesting discussion. C.M. Pandey is thankful to CSIR, India, for the award of SRF.

REFERENCES

1 S. Bose, T. Kuila, M. E. Uddin, N. H. Kim, A. K. T. Lau andJ. H. Lee, *Polymer* 2010, **51**, 5921-5928.

2 D. G. Shchukin, K. Köhler and H. Möhwald, *J. Am. Chem. Soc.* 2006, **128**, 4560-4561.

3 Y. S. Lim, Y. P. Tan, H. N. Lim, W. T. Tan, M. A. Mahnaz, Z. A.Talib, N. M. Huang, A. Kassim and M. A. Yarmo, *J. Appl. Polym. Sci.* 2013**, 128**, 224-229.

4 N. Attarzadeh, K. Raeissi and M. A. Golozar, *Progress in Org. Coat.* 2008**, 63**, 167-174.

Dalton Transactions Accepted Manuscript

5 G. J. Li, L. H. Liu, X. W. Qi, Y. Q. Guo, W. Sun and X. I. Li, *Electrochim. Acta* 2012**,** **63**, 312-317.

6 Y. Tan and K. Ghandi, *Synth. Met.* **2013,** *175*, 183-191.

7 V. Shaktawat, K. Sharma and N.S. Saxena, *J. Ovonic Res* 2010, **6***,* 239–245.

8 D. P. Dubal, S. H. Lee, J. G. Kim, W. B. Kim and C. D. Lokhande, *J. Mat. Chem*. 2012, **22**, 3044-3052.

9 L. Qu, G. Shi, J. Yuan, G. Han and F. E. Chen, *J. Electroanal. Chem.*, 2004, **561**, 149-156.

10 Y. Yang, M. Wan and J. *Mater. Chem*. 2001, **11**, 2022-2027.

11 J. Wang, X. Tao and L. Li, *Synth. Met*. 2014, **194**, 176-181.

12 M. I. Rodriguez and E. C. Alocilja, *IEEE Sens. J.*2005*,* **5***,* 733-736.

13 Z. Gu, L. Zhang and C. Li, *J. Macromol. Sci., Phys.*, *Part B* 2009, **48**, 1093-1102.

14 H. Liu, L. Zhang, Y. Guo, C. Cheng, L. Yang, L. Jiang, G. Yu, W. Hu, Y. Liu andD. Zhu, *J. Mater. Chem. C* 2013, **1**, 3104-3109

15 C. Bora and S. K. Dolui, *Polymer*, 2012, **53**, 923-932.

16 C. Xu, J. Sun and L. Gao, *J. Mater. Chem.* 2011, **21***,* 11253-11258.

17 S. Bose, N. H.Kim, T. Kuila, K.T. Lau and J. H. Lee, *Nanotech.* 2011, **22**, 295202.

18 C. Zhu, J. Zhai, D. Wen andS. Dong, *J. Mater. Chem*. 2012, **22**, 6300–6306.

19 B. Saner, S. A. Gürsel andY. Yurum, *Fullerenes, Nanotubes, Carbon Nanostruct.* 2012*,* **21***,* 233-247.

20 J. Zou, X. H. Song, J. J. Ji, W. C. Xu, J. M. Chen, Y. Q. Jiang, Y. R. Wang and X. Chen, *J. Sep. Sci.* 2011*,* **34**, 2765-2772.

21 N. Prabhakar, P. R. Solanki, A. Kaushik, M. K. Pandey, and B. D. Malhotra, *Electroanalysis*, 2010, **22**, 2672-82.

22 S. Niu, J. Sun, C. Nan andJ. Lin, *Sens. Actuators, B*. 2013, **176**, 58-63.

23 J. Wilson, S. Radhakrishnan, C. Sumathi andV. Dharuman, *Sensors Actuators B,* 2012, **171***,* 216–222.

24 Y. Guo, J. Chen and G. Chen, *Sens. Actuators, B.* 2013, **184**, 113-117.

25 S. Radhakrishnan, C. Sumathi, A. Umar, S. J. Kim, J. Wilson and V. Dharuman, *Biosens. Bioelectron.* 2013, **47**, 133-140.

Dalton Transactions Accepted Manuscript

26 F. Kuralay, A. Erdem, S. Abacı, H. Özyörük and A. Yıldız, *Anal. Chim. Acta,* 2009, **643**, 83-89.

27 K.J. Huang, Y.J. Liu, H.B. Wang, Y.Y. Wang and Y.M. Liu, *Biosens. Bioelectron.* 2014**, 55***,* 195-202.

28 G.J. Li, L.H. Liu, X.W. Qi, Y.Q. Guo, W. Sun and X.L. Li, *Electrochim. Acta* 2012, **63**, 312-317.

29 W. S. Hummers and R. E. Offeman, *J. Am. Chem. Soc*. 1958**, 80** , 1339-1339.

30 I. Tiwari, M. Singh, C. M. Pandey andG. Sumana, *Sens. Actuators, B*, 2015, **206**, 276-283.

31 C. Zhu, J. Zhai, D. Wen and S. Dong, J. *Mater. Chem.* 2012**, 22**, 6300-6306.

32 D. P. Dubal, S. H. Lee, J. G. Kim, W. B. Kim and C. D. Lokhande, *J. Mater. Chem.* 2012**, 22**, 3044-3052.

33 M. Kassaee, E. Motamedi and M. Majdi, *Chem. Eng. J.* 2011, **172***,* 540-549.

34 Y. S. Lim, Y. P. Tan, H. N. Lim, W. T. Tan, M. A. Mahnaz, Z. A. Talib, N. M. Huang, A. Kassim and M. A. Yarmo, *J. Appl. Polym. Sci.* 2013**, 128**, 224-229.

35 K. N. Kudin, B. Ozbas, H. C. Schniepp, R. K. Prud'homme, I. A. Aksay and R. Car, *Nano Lett*. 2008, **8**, 36-4

36 Song, M.; Yu, L. and Wu, Y., *J. Nano Mat.* 2012**,** 5.

37 G. Zhiguo, Y. Shuping, L. Zaijun, S. Xiulan, W. Guangli, F. Yinjun and L. Junkang, *Anal. Chim. Acta* 2011**, 701**, 75-80.

38 L. Qu, G. Shi, J. Yuan, G. Han and F. E. Chen, *J. Electroanal. Chem.* 2004, **561**, 149-156.

39 S. Kumar, S. Kumar, S. Srivastava, B. K. Yadav, S. H. Lee, J. G. Sharma, D. C. Doval, and B. D. Malhotra, *Biosen. Bioelectron.* 2015, **73**, 114–122.

40 C. Basavaraja, W. J. Kim, D. G. Kim and D. S. Huh, *Mater. Chem. Phys.* 2011, **129** (3), 787–793.

41 M. Yang, Y. Yang, H. Yang, G. Shen andR. Yu, *Biomaterials* 2006**, 27**, 246-255.

42 C. M. Pandey, A. Sharma, G. Sumana, I. Tiwari and B. D. Malhotra, *Nanoscale*, 2013**, 5**, 3800-3807.

Dalton Transactions Accepted Manuscript

43 A. Sharma, C. M. Pandey, G. Sumana, U. Soni, S. Sapra, A. K. Srivastava, T. Chatterjee and B. D. Malhotra, *Biosens. Bioelectron.* 2012, **38**, 107-113.

44 A. Erdem, K. Kerman, B. Meric and M. Ozsoz, *Electroanalysis* 2001, **13**, 219-223.

45 A. Erdem, K. Kerman, B. Meric and M. Ozsoz, *Turk. J. of Chem.* 2002**, 26**, 851-862.

46 Ó. A. Loaiza, S. Campuzano, M. Pedrero and J. M. Pingarrón, *Talanta* 2007, **73**, 838-844.

47 A. Lermo, E. Zacco, J. Barak, M. Delwiche, S. Campoy, J. Barbé, S. Alegret and M. I. Pividori, *Biosens. Bioelectron*. 2008, **23**, 1805-1811.

48 X. Mao, L. Yang, X.L. Su and Y. Li, *Biosens. Bioelectron*. 2006, **21**, 1178-1185.

49 Jiang, D. Liu, F. Liu, C. Liu, L. andPu, X. *Int. J. Electrochem. Sci*. **2013**, *8*, 9390 - 9398 O157:H7.

50 S.S. Zhang, Q.Q. Tan, X.M. Li andF. Li, *Sens. Actuators, B,* 2008**, 128**, 529-535.

51 N. Zhou, T. Yang, C. Jiang, M. Du and K. Jiao, *Talanta* 2009*,* 77, 1021-1026.

52 W. Zhang, C. Luo, L. Zhong; S. Nie, W. Cheng, D. Zhao and S. Ding, *Microchim Acta* 2013, **180**, 1233–1240.

53 C. M. Pandey, R. Singh, G. Sumana, M. K. Pandey and B. D. Malhotra, *Sens. Actuators, B,* 2011, **151**, 333-340.

54 C. A. Togo, V. C. Wutor, J. L. Limsonand B. I. Pletschke, *Biotechnol. Lett.* 2007, **29**, 531.

55 C. M. Pandey, G. Sumana and B. D. Malhotra, *Biomacromolecules*, 2011, **12**, 2925-2932.

Dalton Transactions Accepted Manuscript

FIGURE CAPTIONS

Scheme 1. Steps showing the synthesis and electrodeposition of GO-GNPs/PPY nanocomposite.

Figure 1. SEM images of PPY at scan rates (mV/s): (a) 20; (b) 50; (c) 100; (d) 200. Inset: SEM image of PPY at higher magnification

Figure 2. SEM image of (a) PPY inset to Figure: at higher magnification (b) GO-GNPs/PPY hybrid nanocomposite at scan rate 50 mV/s and inset to Figure: of the composite at higher magnification, and (c) pDNA immobilized on GO-GNPs/PPY hybrid nanocomposite.

Figure 3. TEM image of (a) PPY; (b) GO-GNPs; (c) GO-GNPs/PPY nanocomposite ; (d) EDAX analysis of GO-GNPs/PPY nanocomposite; Inset to figures: shows the diffraction patterns of Pure PPY (inset a), GO-GNPs (inset b) and GO-GNPs/PPY nanocomposite (inset c).

Figure 4. FTIR spectra of GO (curve (i)), GO-GNPs (curve (ii)), PPY (curve (iii)) and GO-GNPs/PPY (curve (iv))

Figure 5. CVs of (i) PPY/ITO, (ii) GO/PPY/ITO, (iii) GNPs/PPY/ITO, and (iv) GO-GNPs/PPY/ITO electrode, and (v) pDNA/GO-GNPs/PPY/ITO bioelectrode in phosphate buffer (50mM, pH 7.0, 0.9% NaCl) containing 5 mM $K_3[Fe(CN)_6]^{3-/4-}$].

Figure 6. **(a)** Differential pulse voltametric studies for detection of hybridization at the pDNA/GO-GNPs/PPY/ITO bioelectrode at pulse height of 50mV and pulse width of 70 ms, after methylene blue (MB, 20 μM) pretreatment at +0.1V for 60 s in 0.05M phosphate buffer of pH 7.0 containing 0.153M NaCl. **(b)** Calibration plot for the peak current of MB reduction vs logarithm of concentration of target DNA.

Dalton Transactions Accepted Manuscript

Scheme 1.

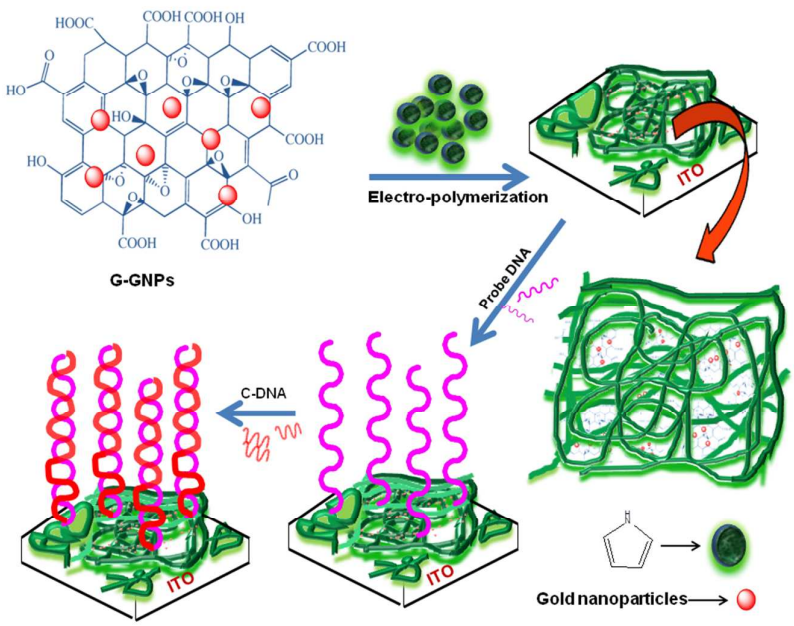

Figure 1.

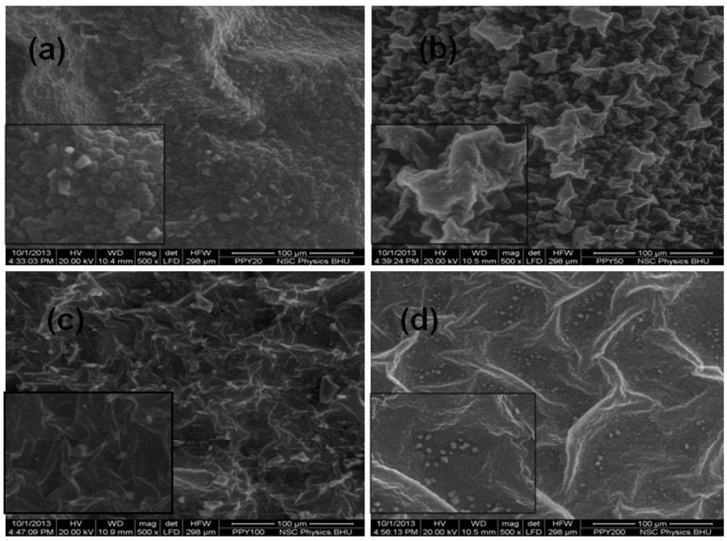

Dalton Transactions Accepted Manuscript

Figure 2.

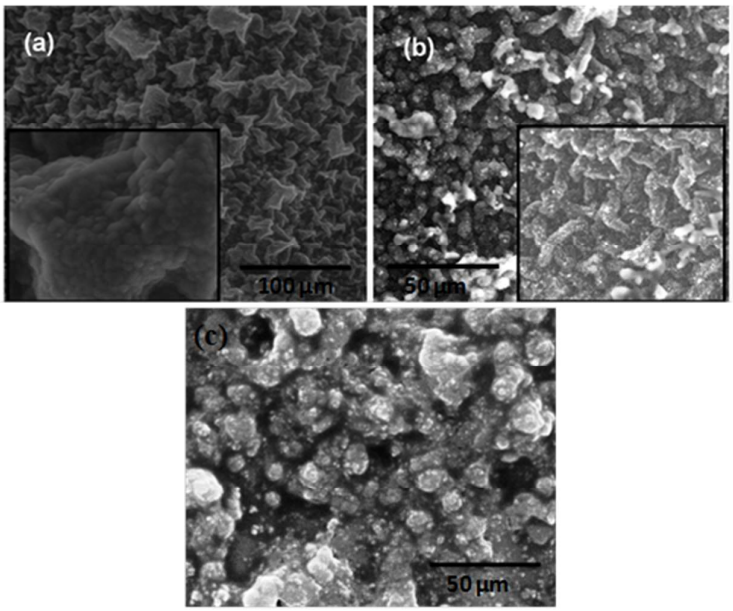

Figure 3.

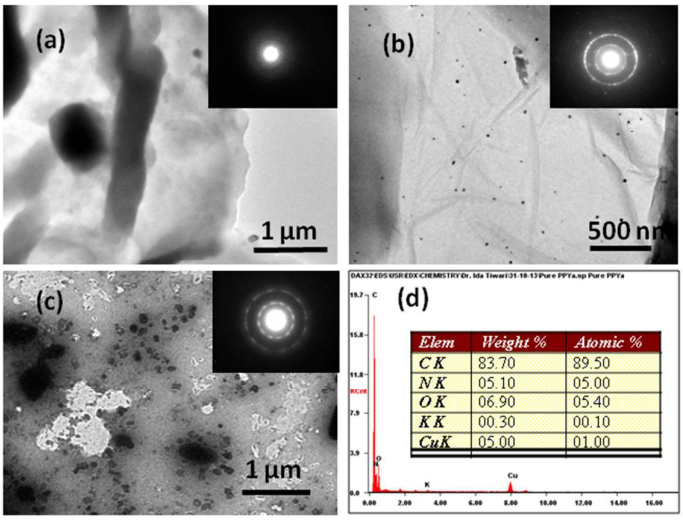

Elem	Weight %	Atomic %
CK	83.70	89.50
NK	05.10	05.00
OK	06.90	05.40
KK	00.30	00.10
CuK	05.00	01.00

Dalton Transactions Accepted Manuscript

Figure 4.

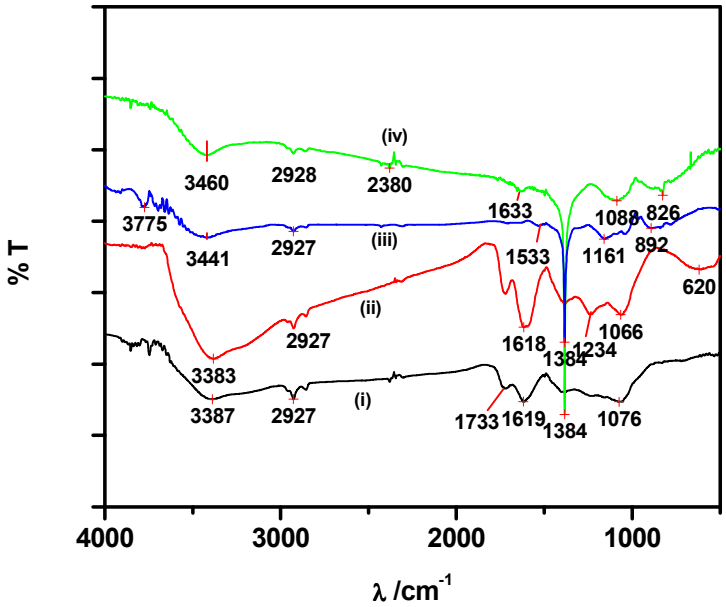

Figure 5.

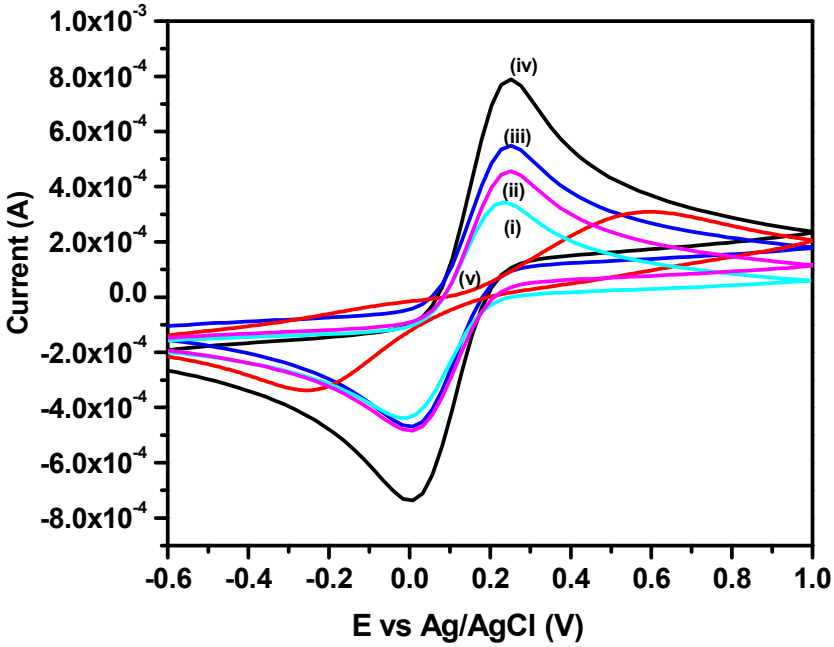

Dalton Transactions Accepted Manuscript

Figure 6.

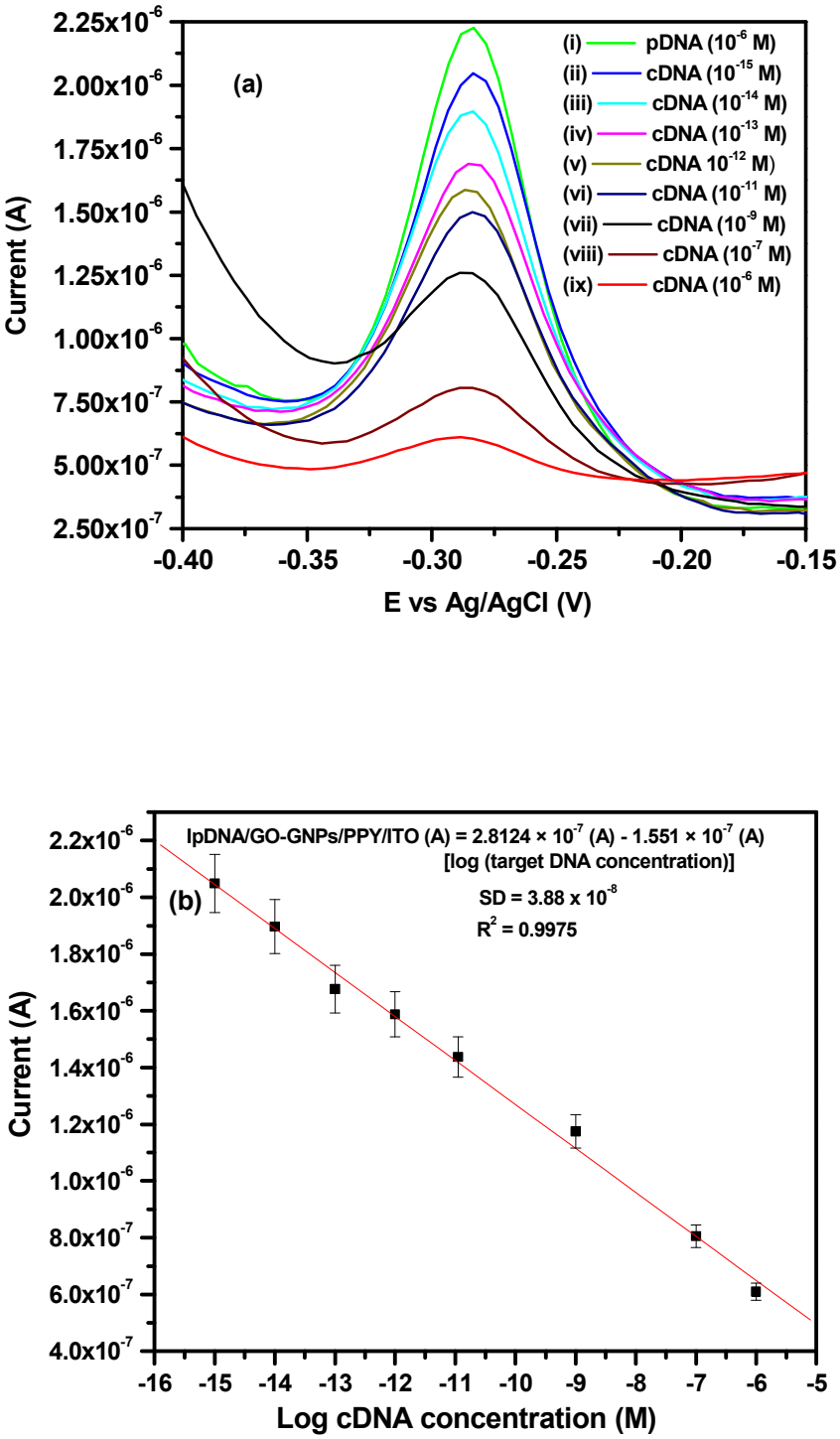

Dalton Transactions Accepted Manuscript

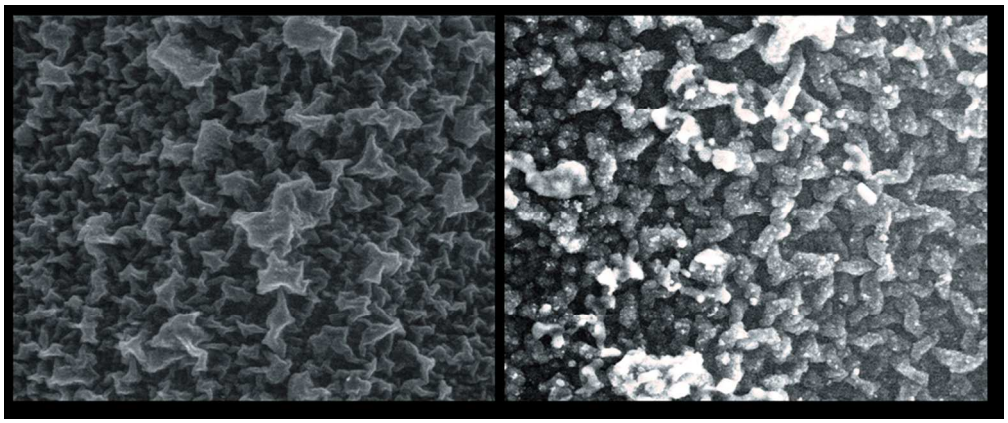

237x87mm (101 x 113 DPI)

Dalton Transactions Accepted Manuscript